Click Here
for
Full
Article

Heterogeneous deformation in the Cascadia convergent margin and its relation to thermal gradient (Washington, NW USA)

Guillermo Booth-Rea,[1] Dirk Klaeschen,[2] Ingo Grevemeyer,[2] and Tim Reston[3]

[1] We combine structural balancing with thermal and strength-envelope analysis of the Cascadia accretionary wedge to determine the influence thermal gradient has on the structure of the prism. BSR-derived heat flow in the Cascadia accretionary margin decreases from $90-110$ mW/m^2 at the deformation front to $45-70$ mW/m^2 in the upper slope. Extension of the thermal gradient to the top of the oceanic crust shows that the base of the prism reaches temperatures between $150-200°C$ and $250-300°C$ at the deformation front and the base of the upper slope, respectively. This high thermal gradient favors the development of a vertical strain gradient, which is accommodated by heterogeneous deformation of the accretionary prism. This process produces two overlying thrust wedges, a basal duplex and an overlying landward- or seaward-vergent imbricate stack. The thermal structure also influences the deformation distribution and structural style along the shortening direction. Initiation of plastic deformation at the base of the prism below the Cascadia upper slope affects the wedge geometry, changing its taper angle and favoring the development of a midcrustal duplex structure that propagates seaward as a dynamic backstop. Uplift related with this underplating process is accompanied with deep incision of submarine canyons, sliding and normal faulting in the upper slope. Heterogeneous deformation accommodated by the development of transfer faults separating landward-vergent from seaward-vergent domains is also observed along the margin. Landward-vergent areas accommodate $30-40\%$ shortening at the front of the wedge, while in the narrower and thicker seaward-vergent segments shortening occurs mostly by underplating below the upper slope. **Citation:** Booth-Rea, G., D. Klaeschen, I. Grevemeyer, and T. Reston (2008), Heterogeneous deformation in the Cascadia convergent margin and its relation to thermal gradient (Washington, NW USA), *Tectonics*, 27, TC4005, doi:10.1029/2007TC002209.

1. Introduction

[2] One key feature which differentiates the Cascadia accretionary margin (Figure 1) from many other subduction zones is its high thermal gradient, which is related to both the young age of the underthrusting Juan de Fuca oceanic plate [*Wilson*, 1993] and the thick (approximately 2.5 km) sedimentary cover entering the accretionary wedge at the deformation front [*Flueh et al.*, 1998]. The thick sedimentary cover acts as an insulating low conductivity layer inhibiting advective heat transfer [*Zhang*, 1993], which in turn results in anomalously high temperatures at the plate interface [*Davis et al.*, 1990; *Hyndman and Wang*, 1993]. Temperature is believed to control whether the subduction interplate zone is seismogenic, with an updip, low-temperature limit at approximately 150°C controlled by diagenetic healing processes [e.g., *Moore and Saffer*, 2001], and a downdip limit between $300-350°C$ related to the P-T dependent onset of quartz plasticity or more unlikely at temperatures of $400-450°C$ if the decollement is of a feldspathic composition [e.g., *Brace and Byerlee*, 1970; *Hyndman and Wang*, 1993; *Scholz*, 1998; *Oleskevich et al.*, 1999]. The entire subduction plane in the Cascadia margin is at temperatures above 150°C, forming a wide locked seismogenic zone bounded landwards by the $300-350°C$ isotherm [*Hyndman and Wang*, 1993, 1995; *Oleskevich et al.*, 1999; *Gutscher and Peacock*, 2003].

[3] Temperature is one of the most important variables for activating the main ductile deformation mechanisms in rocks, favoring diffusion and solubility. It appears as an exponent in the main rock flow laws, such as in dislocation creep [e.g., *Brace and Kohlstedt*, 1980; *Kohlstedt et al.*, 1995; *Hirth et al.*, 2001; *Wintsch and Yi*, 2002; *Rybacki and Dresen*, 2004]. Temperature is also important at larger scale, influencing the structure of orogenic wedges. The Coulomb critical taper model has been extended to include the effects of temperature-dependent plastic deformation [*Williams et al.*, 1994], predicting changes in the wedge geometry related with the temperature reached at the basal decollement and at the base of the wedge. Temperature, however, is not a variable considered in analogue wedge models, probably, because of the difficulty of scaling temperature-dependent processes with the materials used for modeling. Thus rheological ductile behaviors for modeling ductile-brittle wedges are obtained using ductile materials such as silicone putty instead of varying the temperature [e.g., *Couzens-Schultz et al.*, 2003; *Smit et al.*, 2003; *Bonini*,

[1]Departamento de Geodinámica, Universidad de Granada, Campus de Fuentenueva, Granada, Spain.
[2]IFM-GEOMAR, Leibnitz Institute of Marine Sciences, Kiel, Germany.
[3]School of Geography, Earth and Environmental Sciences, University of Birmingham, Birmingham, UK.
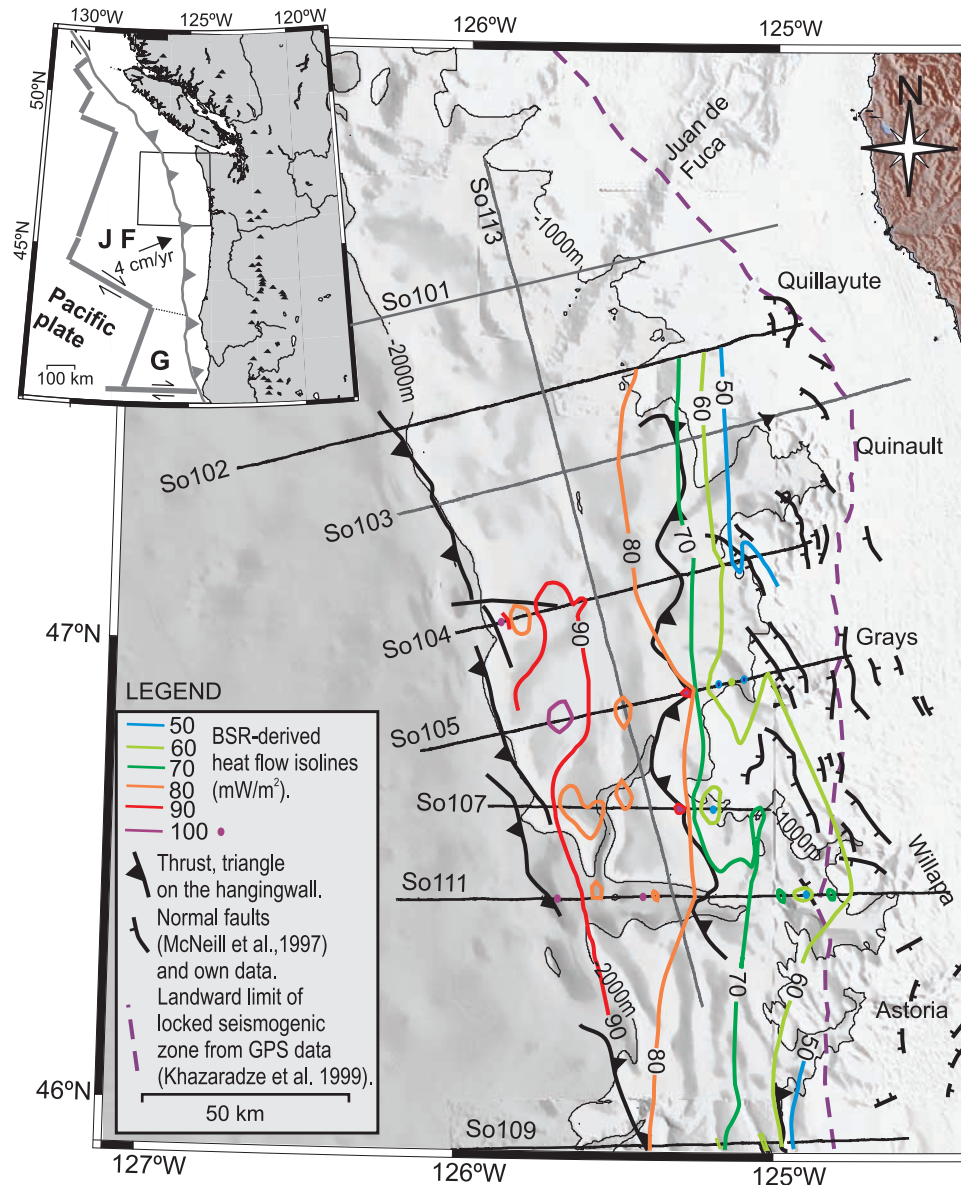
Figure 1. Tectonic setting of the Cascadia convergent margin and location of the So108 seismic lines. Notice mostly landward vergence at the toe of the accretionary wedge and the seaward vergent thrust defining a morphologic scarp at the base of the Cascadia upper slope. The BSR-derived heat flow, the landward limit of the locked seismogenic zone and normal faults affecting the Cascadia shelf and upper slope have also been illustrated. Inset shows location of the Cascadia trench-arc system, JF-Juan de Fuca plate, G-Gorda plate; triangles are active volcanoes. Bathymetry from USGS [*Haugerud*, 1999] (http://geopubs.wr.usgs.gov/open-file/of99-369).

2007]. The effects of temperature in the structure of orogenic wedges are thus generally addressed from a theoretical point of view by thermomechanical modeling [e.g., *Williams et al.*, 1994; *Burov et al.*, 2001; *Bollinger et al.*, 2006] or empirically by thermomechanical field data analysis [e.g., *Dunlap et al.*, 1997]. Here we will analyze and discuss the influence the temperature field has in the structure of the Cascadia margin using geophysical data and structural balancing analysis.

[4] The Cascadia margin is a classical example of a purely accretionary margin where most of the sedimentary cover is scraped off the oceanic crust by frontal accretion, leading to the formation of a landward-vergent imbricated fan [e.g., *MacKay*, 1995; *Flueh et al.*, 1998; *Gutscher et al.*, 2001]. Different mechanical models have been used to explain the structure of the Cascadia margin, especially, the presence of the landward-vergent imbricate fan developed in the frontal part of the wedge in regions close to the Astoria and Ninifat submarine fans. These models commonly require atypical physical conditions like viscoelastic non-Coulomb rheological behavior, a high basal subduction angle or specific backstop geometries. *Seely* [1977] and

Byrne et al. [1993] suggested that landward vergence was related with a weak basal fault, related to high fluid pressures. *MacKay* [1995] emphasized that some additional mechanism was necessary to produce the landward imbricate fan, either lithological, related with a mechanically strong wedge relative to the basal thrust or a high-dipping angle at the base of the wedge. Analogue model studies suggest that the formation of the landward vergent imbricate fan required extreme non-Coulomb conditions at the base of the wedge, supposedly related to the presence of carbonate-rich oozes, which were modeled using a Newtonian rheology [*Gutscher et al.*, 2001]. The distribution and concentration of smectite, which reduces basal friction and contributes to the development of high fluid pressures when it dehydrates, has also been considered as the main mechanism determining the distribution of landward- and seaward-vergent areas along the margin *Underwood* [2002].

[5] A mechanical model was proposed for the frontal part of the Cascadia prism by *Adam et al.* [2004] that does not require any extreme rheological properties, and relates the structure of the prism to vertical strain partitioning in the wedge. This model proposes the existence of a seaward-vergent duplex at the base of the wedge, above which, the landward imbricate fan roots. According to these authors the activation of deformation of this style was triggered by a strong increment in Pleistocene sedimentation rates related to glaciations; a process that increased lithostatic loading and fluid pressures at the base of the accretionary wedge.

[6] We present prestack depth migrated seismic lines acquired during the ORWELL Cruise with R/V SONNE in 1996 [*Flueh et al.*, 1998; *Fisher et al.*, 1999] across the Cascadia margin offshore Washington (Figure 1). These lines were balanced and restored to the undeformed state, showing the geometry and amount of shortening along the margin. These lines also image bottom simulating reflectors (BSR) that are widespread in most of the Cascadia continental slope. BSR-derived heat flow was used to determine the temperature gradient between the surface and the base of the wedge. Superposition of the thermal gradient to the structure of the accretionary wedge, together with the calculation of a few strength envelopes along the wedge permits us to understand some of the thermally activated processes that occur in the Cascadia margin and their bearing on its structure and tectonic evolution. Finally, we discuss the influence that lithological and sedimentary thickness variations may have in the heterogeneous deformation along the margin, specifically, relative to the position of the Cascadia submarine fans.

2. Tectonic Setting and the ORWELL Seismic Lines

[7] Subduction of the Juan de Fuca oceanic crust, with an age between 4 and 12 Ma [*Wilson*, 1993; *Govers and*

Meijer, 2001], occurs beneath North America in the Cascadia margin. This subduction zone is characterized by moderate convergence rates (4.3 cm/a toward the ENE) [*Engebretson et al.*, 1983; *DeMets et al.*, 1990, Figure 1]. Furthermore, it shows a very low subduction angle between 2 and 12° at the subduction front and below the continental shelf, respectively [*Trehu et al.*, 1994; *Flueh et al.*, 1998; *Gutscher and Peacock*, 2003]. The Orwell seismic lines show the structure of an important area of the Cascadia margin between parallels 48°N and 46°N [*Flueh et al.*, 1998; *Fisher et al.*, 1999; *Gutscher et al.*, 2001; *Adam et al.*, 2004] (Figure 1). Most of the lines, each more than 120 km long, were shot approximately along the convergence direction (So101, 102, 103, 104, 105, 107, 111, and 109). An additional line (So113) was shot parallel to the margin crossing all the margin-normal lines except So 109 (Figure 1).

[8] The seismic lines acquired to the north of parallel 46.5°N image a landward-vergent imbricate fan in the frontal part of the accretionary wedge (first 40–50 km) that developed during the Pleistocene [*Barnard*, 1973; *Flueh et al.*, 1998; *Adam et al.*, 2004]. This Pleistocene part of the wedge forms a terrace above the Juan de Fuca abyssal plain with a very low slope angle, between 1–2°, bounded by the deformation front oceanward and by the upper slope toward the continent. The upper slope shows a higher surface angle between 3–5° and is bounded landwards by the continental shelf. The higher angle of the upper slope has favored incision and backward erosion of submarine canyons, the development of listric normal faults [*McNeill et al.*, 1997] and submarine slides [*Goldfinger et al.*, 2000] (Figures 1 and 2).

[9] The sedimentary infill of the Cascadia basin is formed by three stratigraphic units, well differentiated by their seismic velocities [*Flueh et al.*, 1998]. The basal unit, overlying the oceanic crust, is formed by hemipelagic sediments [*Duncan and Kulm*, 1989; *Underwood*, 2002], sometimes with a carbonate-rich fraction, characterized by high seismic velocities of up to 3.5 km/s and showing a rather constant thickness between 600 and 800 m. This unit is covered by a thick succession of Plio-Pleistocene turbidites [*Duncan and Kulm*, 1989]. Two subunits have been differentiated in the turbidites, a deeper one formed by distal silty turbidites and a shallow one formed by fine to medium sandy turbidites. The distal turbidites are characterized by intermediate velocities (2.5–2.9 km/s), while the overlying turbidites show intermediate to low velocities (2.2 to 2.5 km/s) [*Adam et al.*, 2004]. The turbidite units show great thickness variations, doubling their thickness toward the continent. Related to the imbricate thrust systems there are many small asymmetric basins developed on the thrust footwalls, filled by low-velocity Pleistocene to Holocene sediments (1.7 a 2.1 km/s) [*Adam et al.*, 2004].

[10] The vast majority of the sedimentary cover of the Cascadia basin, deposited above the Juan de Fuca plate, is incorporated to the accretionary wedge at the deformation

Figure 2. Structural interpretation of seismic profile So107, characteristic of areas with landward vergence in the Cascadia margin. The areas enlarged below show good examples of the BSR picked for determining the heat flow in the margin.
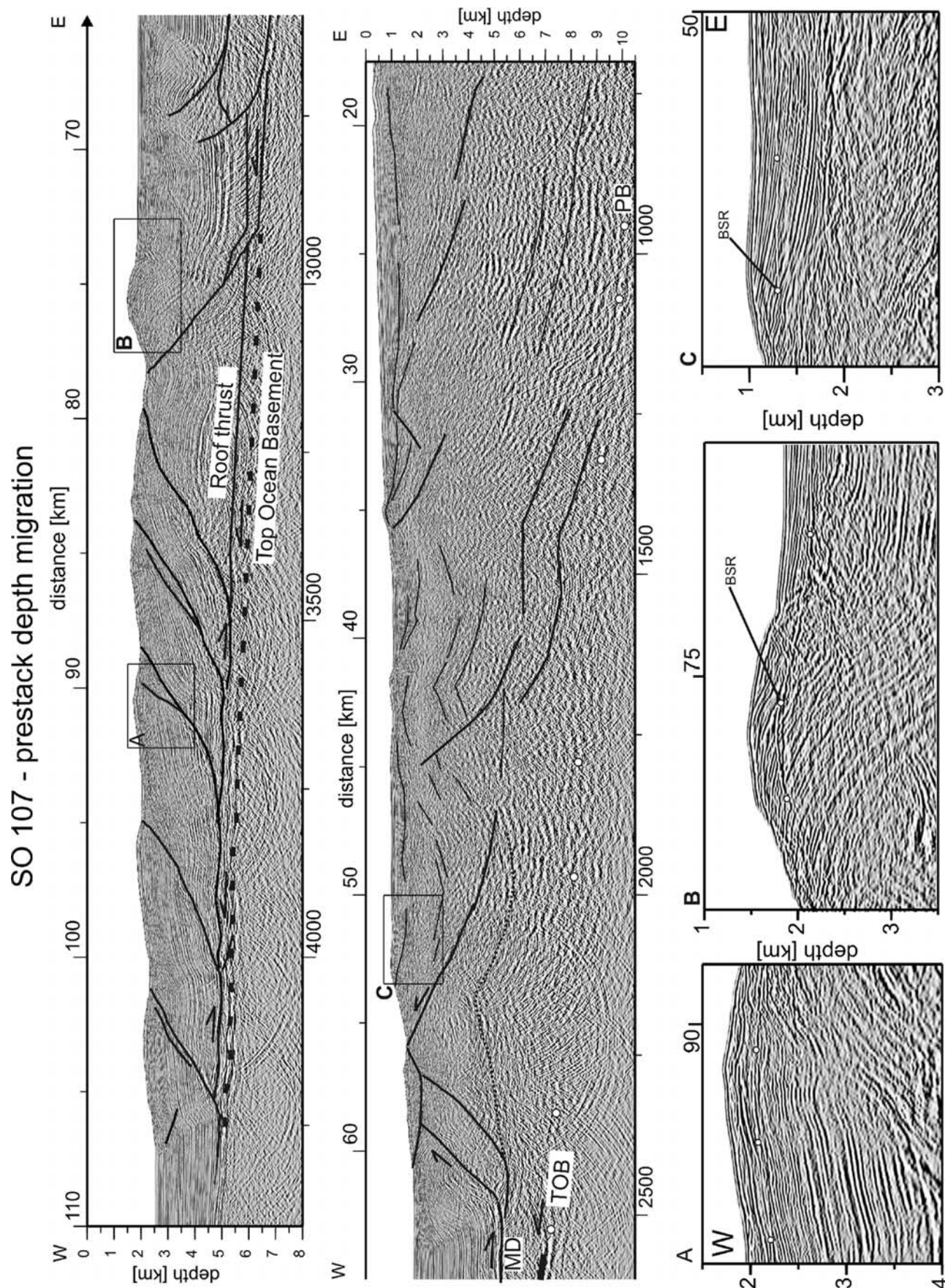
Figure 2

front, where the sediments reach a thickness between 2.5 and 4 km (Figures 2 and 3), with the thicker sequences occurring along the central axis of the Astoria submarine fan (Line So109). This thicker sedimentary sequence imaged by line So109 is deformed by a seaward-vergent imbricate fan that contrasts with the structure imaged to the north.

[11] The ORWELL seismic lines were processed in IFM-GEOMAR (Kiel, Germany). Processing of the seismic lines included iterative prestack-depth migration taking into consideration velocity data obtained from refraction seismics obtained during the same cruise [*Flueh et al.*, 1998]. Using the refraction data to start with permitted to optimize the depth resolution. The resulting depth migrated lines image the structure of the prism without the distortion that occurs in time sections, and is thus ideal for structural balancing analysis. Depth migration resolves the actual sediment seismic velocities, hence, facilitating the determination of other sediment physical properties like porosities [e.g., *Adam et al.*, 2004].

3. Structure of the Cascadia Margin Offshore Washington

[12] Structural analysis of the Cascadia accretionary prism included balancing and restoring the deformed strata imaged on the prestack depth-migrated seismic lines. The structural balancing and restoration was carried out using GEOSEC software. This balancing software takes in consideration the conservation of both areas and lengths of material lines between the deformed and undeformed states. The restored shortening in the accretionary wedge is obviously subject to errors, which are difficult to evaluate, related to the existence of internal heterogeneous strain, deformation out of the X-Z convergence plane and homogeneous horizontal shortening. However, there seems to be a reasonable fit between the balanced and imaged seismic structure, thus, balancing greatly helps to define the detail geometry of the main thrusts in the prism and to measure the shortening associated to thrusting.

[13] Heterogeneous deformation in the Cascadia margin occurs in three perpendicular directions: parallel to the convergence direction, in depth and parallel to the margin. It is expressed at different scales, from the development of strain gradients within a single thrust sheet, to changes in the structural style within the accretionary wedge or in the amount of shortening along the margin. Strain partitioning at the scale of a single thrust sheet is especially evident in the first thrust, at the deformation front. Here the dip of the limb formed by the hangingwall flat, folded by fault bending above the underlying footwall ramp, increases at depth, indicating the existence of a vertical strain gradient at the base of the thrust sheet (Figure 4). This vertical strain gradient is manifested also by a large downward decrease in porosity in the sedimentary sequence [*Adam et al.*, 2004]. Furthermore, small-scale reverse faulting is only observed in the shallower parts of the thrust sheet, suggesting a change in the main deformation mechanism at depth (Figure 4).

[14] At a larger scale, deformation partitioning in the frontal part of the accretionary wedge, in areas where the landward imbricate thrust fan developed, resulted in the superposition of two thrust wedges. These thrust wedges are a basal hinterland-dipping duplex (basal duplex) and an overlying landward-vergent imbricate thrust fan that detaches on the duplex roof thrust. This roof thrust is a flat detachment that partitions the deformation between the base and the surface of the accretionary wedge [*Adam et al.*, 2004, Figures 2 and 5]. The position of the core-duplex roof thrust coincides approximately with a mechanical discontinuity between the basal hemipelagic sediments and the overlying turbidites.

[15] Along the central axis of the Astoria submarine fan, the accretionary wedge is deformed by a seaward-vergent imbricate thrust fan that also detaches on a flat-lying thrust. This thrust lies close to the oceanic crust at the deformation front, but separates from it toward the margin, bounding an underlying wedge that may represent a duplex, which in this case would have the same vergence as the overlying thrust imbricate fan (Line So109, Figure 3).

[16] These changes in the structural style of the frontal part of the prism along the margin are accompanied also by differences in the wedge taper angle, in the geometry of the thrusts and in the amount of shortening (Figure 6). In the northern area, the frontal part of the wedge has a very low surface angle of approximately 1° (lines So104, 105, and 111); while along line So109 the surface angle is of 2°. The thrusts in the northern segment dip between 38 and 25° and sometimes have ramp-flat geometries (lines So104, 105, 107, and 111). In line So109 the thrusts show dips of up to 53°, being thus reverse faults. They are planar along most of their length and have a listric geometry at depth. Probably the most dramatic contrast between the two imbricate thrust fans is the amount of shortening they accommodate. While the percent of shortening, measured by restoring the frontal part of the balanced sections to the undeformed state in lines So104, So105, So107, and So111, is approximately 30% it is only a third of this in the seaward-vergent imbricate fan imaged in line So109 (11%) (Figure 6).

[17] Along the shortening direction we have observed strong changes in the structural style that have permitted us to divide the accretionary wedge into five different structural domains (Figure 5). From the deformation front toward the continent these are the following.

[18] (1) A frontal domain characterized by the landward-vergent imbricate thrust fan imaged in the northern seismic lines [*Seely*, 1977; *MacKay*, 1995; *Flueh et al.*, 1998; *Fisher et al.*, 1999; *Gutscher et al.*, 2001; *Adam et al.*, 2004].

[19] (2) A triangular zone [*Adam et al.*, 2004] with a N-S orientation located 30 to 35 km from the deformation front that has been imaged in lines So103, 104, 105, 107, and 111. East of the triangular zone the accretionary wedge has normal seaward vergence (Figures 5 and 6).

[20] (3) A zone approximately 20 km wide characterized mostly by detached folds, without thrusts, between the triangular zone and the base of the upper slope (Figure 6). This zone, together with the two previous ones, shows a very low surface angle of approximately 1°. The shallow
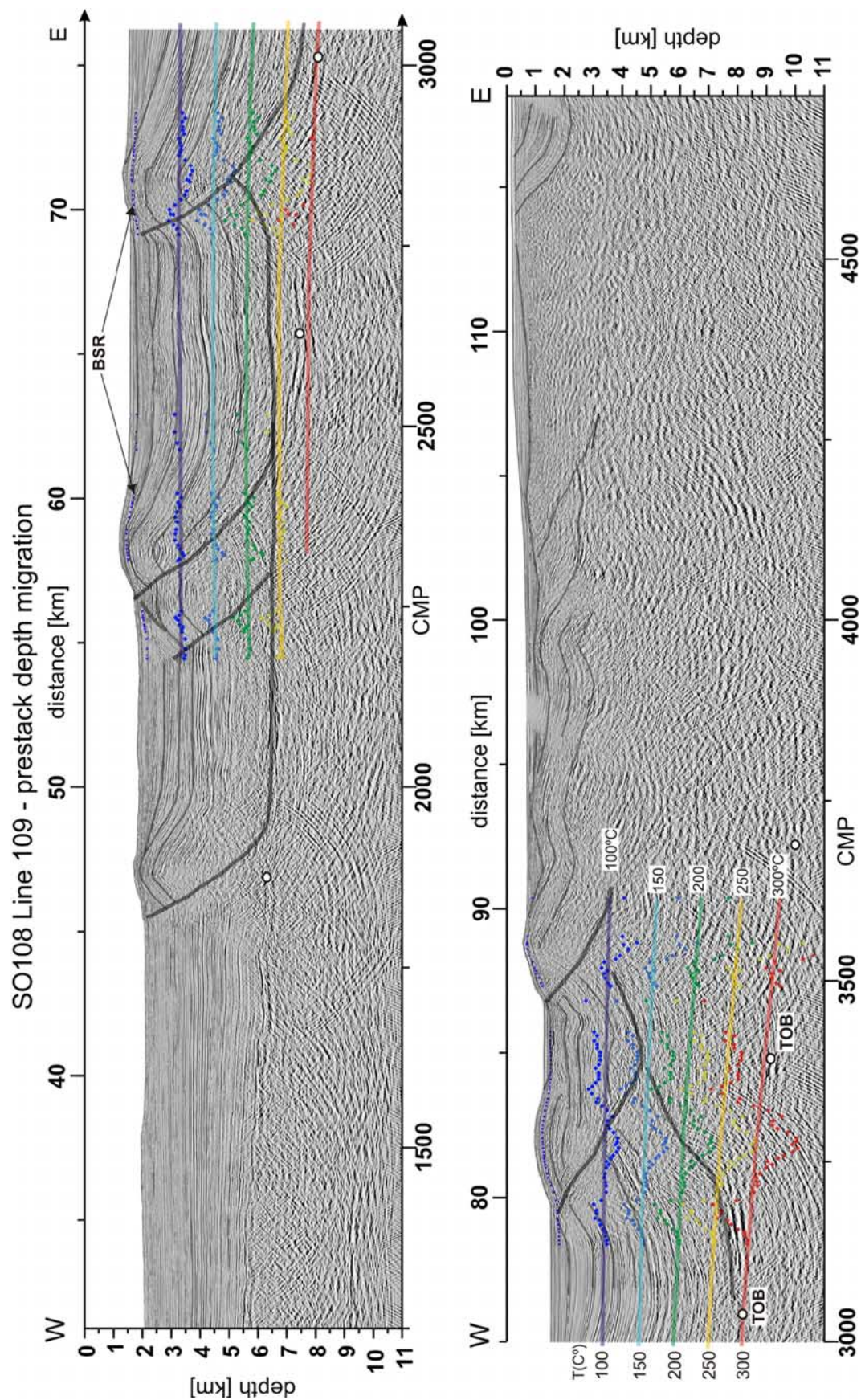
Figure 3. Structural interpretation of seismic profile So109, showing seaward vergence. We have overlain the position of BSR reflections and isotherms determined from BSR-derived heat flow data. The dots represent the temperature results obtained directly from each BSR-derived heat flow point, before fitting to a polynomial curve.
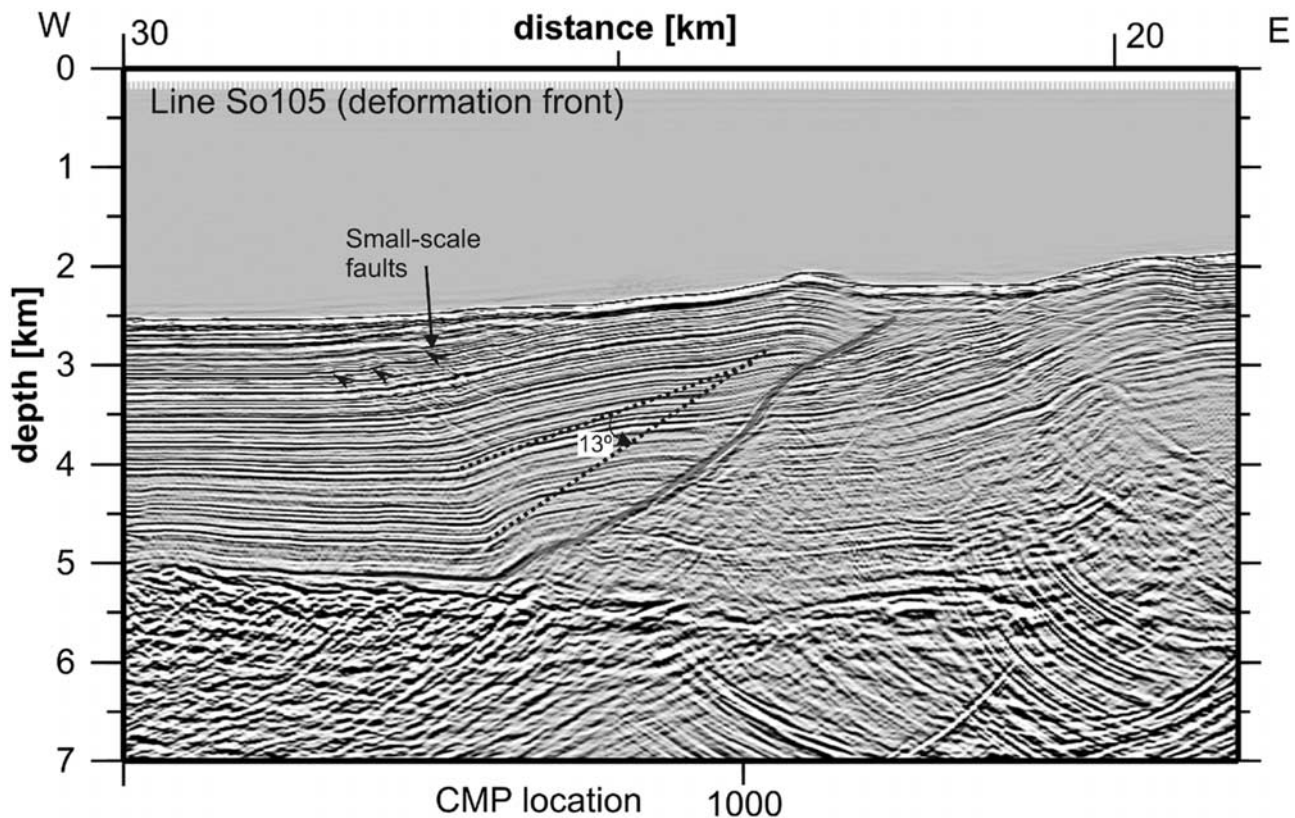
Figure 4. Detail of the deformation front in line So105. This line shows the existence of a strain gradient between the surface and the base of the thrust sheet at the deformation front, together with heterogeneous deformation with brittle faults forming at the surface.

surface angle of this zone may have favored the establishment of the main axial drainage system, the Cascadia channel that runs with an N-S orientation through the submarine valley developed in this domain [e.g., *Underwood et al.*, 2005].

[21] (4) Markedly different is the structure of domain 4 that coincides with the upper slope of the Cascadia margin. First of all the surface slope of the prism increases abruptly to $3-5°$ producing a step 20 to 35 km wide in the bathymetry of the margin. The base of this zone coincides with the trace of an out-of-sequence thrust that has hangingwall-flat geometry, indicating displacements larger than the length of the underlying thrust ramp. We have named this thrust the Cascadia Main Thrust (Figure 5). The landward limit of the upper slope domain is the continental shelf. The bathymetry in this region contrasts with the one observed in the lower-slope terrace and is characterized by deep incision of submarine canyons, submarine slide scars [*Goldfinger et al.*, 2000] and normal fault scarps [*McNeill et al.*, 1997]. The basal-duplex roof thrust is abandoned and warped below the base of the upper slope. This process is observed also to the south in line So109. Many listric normal faults occur in the upper slope domain [Figures 1 and 5, *McNeill et al.*, 1997]. Locally, these faults seem to root in landward-inclined reflections interpreted as thrusts. This feature is especially clear in line So104 (Figure 5) where the normal fault farther offshore roots in the Cascadia Main Thrust. The normal faults are generally, younger oceanward both in the lines studied by *McNeill et al.* [1997] and the ones shown here.

[22] (5) The continental shelf has a very low surface slope, being practically horizontal. All structures have been sealed by recent sediments in this area. Generally, rocks in this domain dip toward the continent suggesting the existence of a system of sealed landward-dipping thrusts with hangingwall flat geometries.

[23] Active deformation of the accretionary prism seems to occur mostly by frontal accretion; however, active shortening could also be taking place along the Cascadia Main Thrust that shows a clear fault line scarp and cuts the bathymetry in most of the margin. Also, in lines So105 and So107 it seems that the seaward-vergent thrust of the triangular zone has been reactivated, now rooting at the plate interface. This thrust has a very prominent anticlinal ridge associated to it and it cuts the entire sedimentary sequence. Furthermore, underplating by duplex formation below the upper slope could also represent a mechanism of active deformation within the accretionary wedge. This seems to be the case in Line So109, where the thrusts present in the upper slope root in a very shallow detachment that has been folded or warped from below.

[24] We plotted the trace of all structures imaged in the seismic lines (So101 to So113) on the bathymetry of the margin. Interpolating the thrust traces, with the aid of a
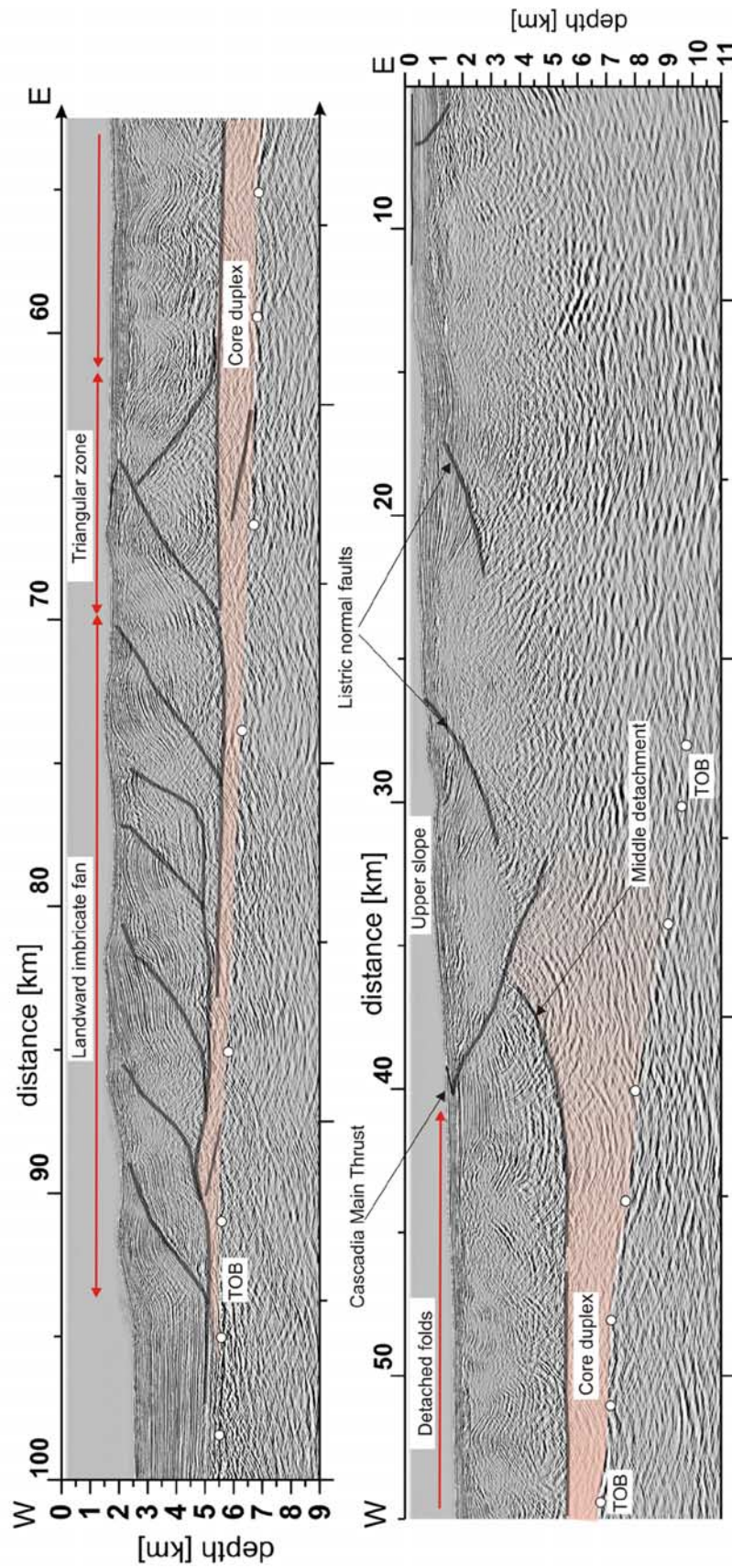
Figure 5. Main structural domains in the landward-vergent region of the Cascadia accretionary wedge as observed in seismic line So104.

Line So104

24% shortening

10 km

0   10   20   30 km

Line So105

26 % shortening

11.5 km

0   10   20   30 km

Line So107

31% shortening

W=E

15.2 km

0   10   20   30 km

Line So111

26% shortening

21 km

0   10   20   30 km

Line So109

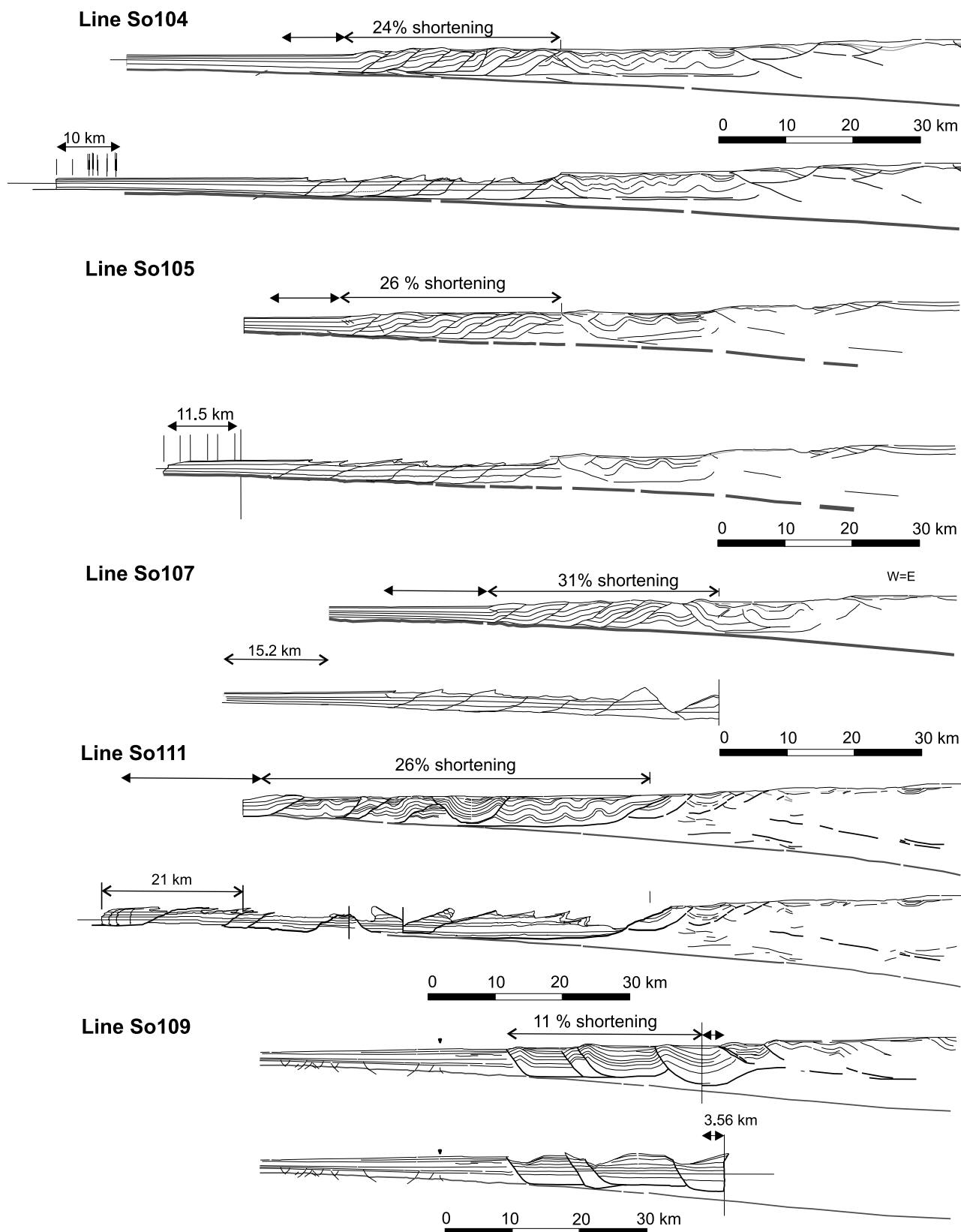11 % shortening

3.56 km

0   10   20   30 km

Figure 6. Structural balancing and restoration of the frontal part of the Cascadia accretionary wedge cut by the seismic lines studied here. Note the changes in structural style from north to south between lines So104 and So109.
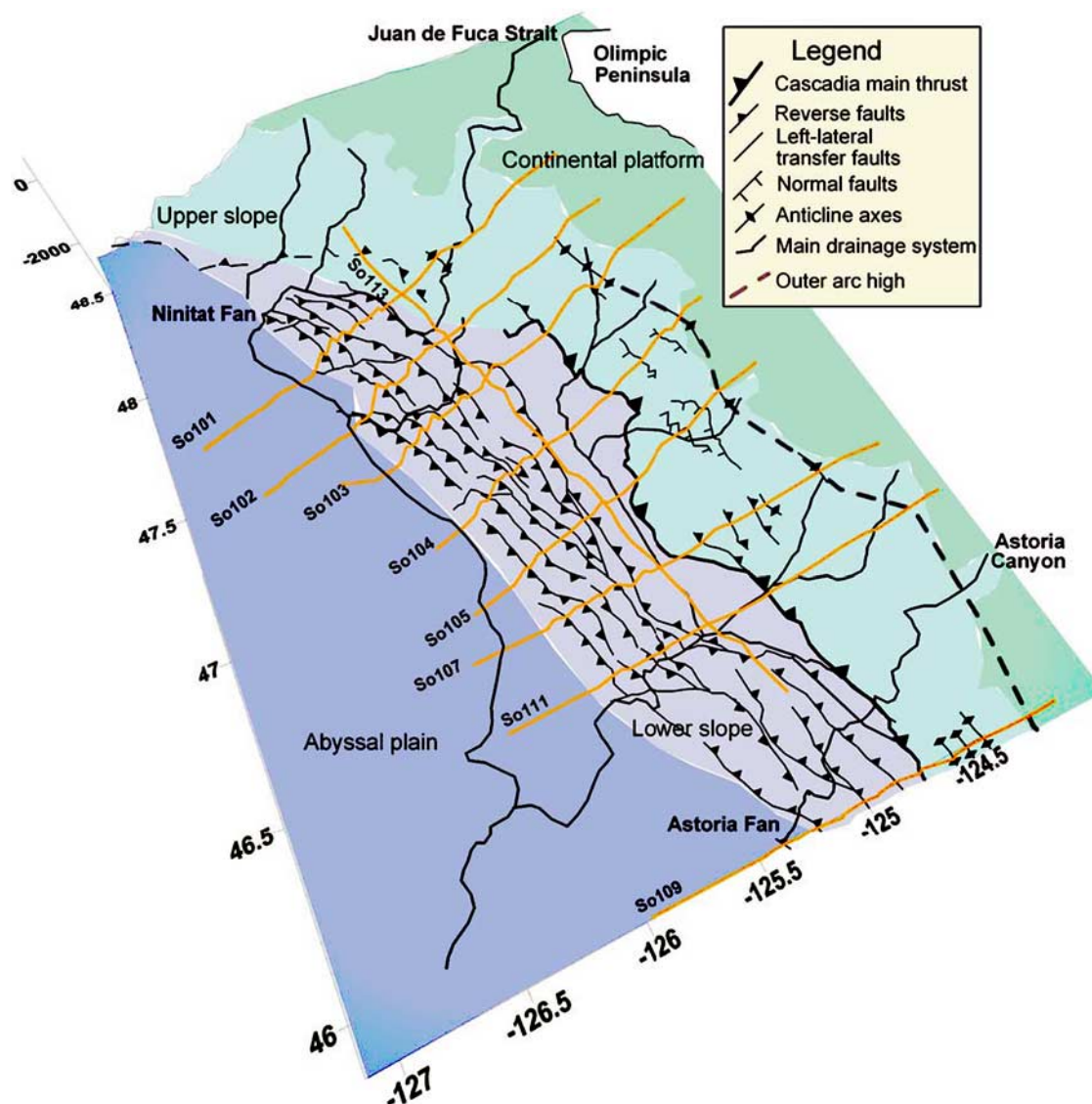
Figure 7. Structural map of the Cascadia convergent margin offshore Washington determined from the seismic lines shot in the ORWEL cruise.

classified and unpublished 250 m bathymetric database, has helped us produce a structural map of the Cascadia margin offshore Washington (Figure 7). This map shows the 3-D relationships between the different thrusts identified in the accretionary wedge and especially the occurrence of lateral transfer faults that accommodate the change of vergence to the north and south of line So111.

4. BSR-Derived Heat Flow and the Accretionary-Wedge Temperature Gradient

[25] Bottom Simulating Reflectors (BSRs) occur discontinuously in most of the Cascadia lower slope and in the lower parts of the upper slope (Figure 2). This has permitted us to estimate the temperature gradient of the prism using the BSR-derived heat flow. The heat flow was determined

following the methodology used by *Davis et al.* [1990] and *Grevemeyer and Villinger* [2001]. We have derived the depth of the BSR directly from the prestack depth migrated sections. The temperature at the BSR was determined from the pressure-temperature stability for methane hydrate under hydrostatic pressures, assuming that the primary composition is methane in seawater [*Dickens and Quinby-Hunt*, 1994]. Thermal conductivity was adopted from *Davis et al.* [1990]. BSR-derived heat flow ranges between 110–80 and 45–70 mW/m^2 at the toe of the accretionary wedge and within the upper slope, respectively (Figures 1 and 8). A heat flow peak is observed at the base of the upper slope in the footwall of the main out-of-sequence thrust, where the heat flow reaches 100 mW/m^2, which is approximately 25 mW/m^2 above the regional trend in this area (Figure 8). Commonly, the heat flow reaches its maximum in the
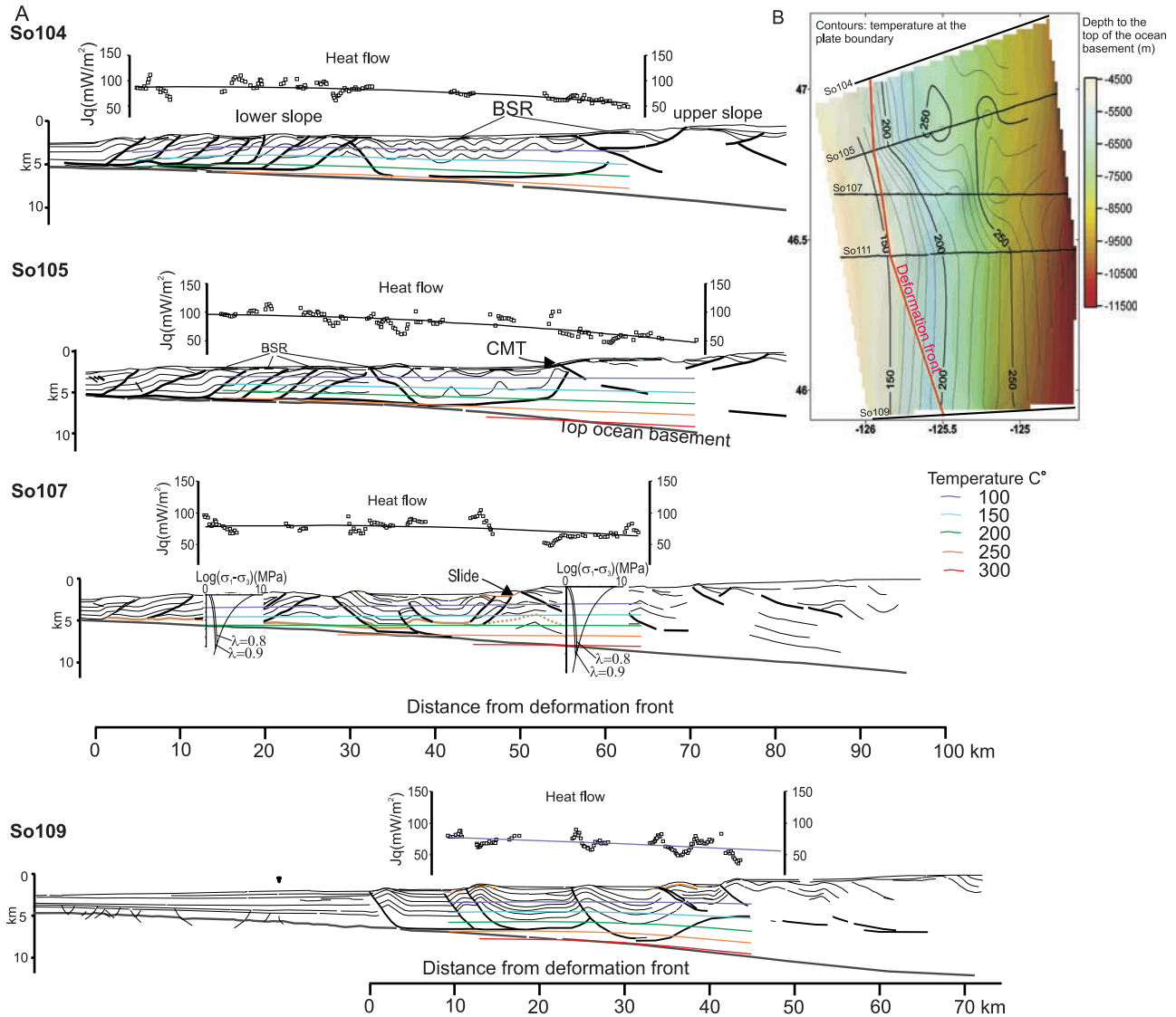
Figure 8. (a) Seismic lines So104, 105, 107, and 109 overlain with BSR-derived heat flow data and thermal field. Two strength envelopes have been plotted on line So107 showing how the plastic-brittle transition occurs at the base of the wedge below the Cascadia upper slope. See text for discussion. (b) Temperature at the plate boundary determined from BSR-derived heat flow, contoured over a grid of the depth to the plate boundary. These isotherms have been determined from heat flow data filtered to fit polynomial lines shown in Figure 8a.

footwall of the thrusts directly below the intersection between the thrusts and the sea bottom and decreases toward the hinges of the anticlinal ridges as described further north by *Ganguly et al.* [2000], Figure 8. The low heat flow results obtained in the upper slope fit well with the average 40 mW/m^2 determined by *Blackwell et al.* [1990] in the Washington forearc coastal provinces.

[26] The temperature gradient was determined using the BSR-derived heat flow, radiogenic heat production (0.65 * 10^{-6} W/m^3) derived from gamma logs of Ocean Drilling Program Sites 1244E and 1245E [*Tréhu et al.*, 2003] and the conductivity model used by *Davis et al.* [1990] in the northern Cascadia accretionary prism, including a constant

value of 1.8 Wm^{-1}K^{-1} at depths greater than one km. Temperature gradient determinations using a higher thermal conductivity of 2.4 Wm^{-1}K^{-1} below 1 km result in displacement of the 300°C isotherm approximately 1.3 km deeper. The sections have been assumed to be in thermal equilibrium and the surface heat flow has been used to extrapolate the temperature field down to the plate boundary. This 1-D approach is probably valid as a first approximation to the upper plate thermal structure. Modeling further down, across the plate boundary would require treating the thermal equilibrium with a dynamical approach [e.g., *Wang*, 2000; *Gutscher and Peacock*, 2003; *Hyndman and Peacock*, 2003]. The temperature results have been

smoothed using a polynomial fit to the data to minimize the effects of topography, active thrusting and fluid advection on heat flow. The temperatures at the plate boundary range between 180–200 and 250–300°C at the deformation front and below the upper-slope break, respectively. Lower temperatures at the plate boundary were obtained in line So104 where the oceanic crust has a lower dip and where the wedge has been partly thinned by listric faults, having a lower surface angle in the upper slope (Figure 8a). Higher temperatures were obtained to the south in line So109, where the wedge taper angle is larger, both because of an increase in the wedge surface angle and the dip of the subducting plate (Figure 8b), thus resulting in a thicker wedge. The thicker wedge in this region is also related to a greater thickness of the incoming sedimentary cover coinciding with the axial zone of the Astoria submarine fan.

5. Strength Envelopes in the Accretionary Wedge

[27] To constrain better the rheological behavior of the rocks imaged in the prism we have calculated several strength envelopes in points that we considered important for understanding the structure of the prism and where we had heat flow data to determine a geotherm. Of the existing rheological models, we have chosen the one determined for dislocation creep in wet quartzites [Ranalli, 1995], which may adjust to the turbiditic sediments of the accretionary wedge (σ_{zz}-$\sigma_{xx} = (\varepsilon/A)^{1/n}\exp(E/nRT)$, where A = $3.2*10^{-4}$ MPa^{-n}s^{-1}, n = 2.3 and E = 154 kJmol^{-1}). Using a weaker rheology like wet granite or a stronger material like plagioclase (An75) produces variations of approximately ±1.5 km in the position of the brittle ductile transition. For determining the frictional deviatoric stress we have used the equation given by the modified Anderson theory ((σ_{zz}-$\sigma_{xx} = \alpha\rho gz(1-\lambda)$). We have used elevated pore pressures (λ = 0.9 and 0.8), required to explain the low surface angle (1–4°) of the prism [Davis et al., 1983]. The increase in slope angle below the upper slope may indicate among other factors a decrease in fluid pressure in this region. Although, previous work has suggested that the development of listric low-angle normal faults in this region required high fluid pressures in the wedge [McNeill et al., 1997]. Finally, the strength envelopes have been determined assuming thrust faulting following the method described by Ranalli [1995].

[28] Deformation rate ε has been calculated assuming that all deformation related to plate convergence (4.5 cm/a) is accommodated by frontal accretion in the prism. We calculated the amount of shortening related to thrusting and added 5–10% more shortening assumed to be produced by homogeneous horizontal layer thickening. The age of the frontal prism was obtained simply by dividing the shortening between the convergence rate, obtaining an age of approximately 400 to 450 kyr for the deformation accumulated in the landward-vergent imbricate fan and the triangular zone in line So107. We measured 15.2 km shortening in the frontal part of line So107 after restoration that represents 30% shortening of this section. If we add 5–10% shortening related with horizontal layer thickening, we

obtain 18 to 20 km of shortening equivalent to an extension (e = $\Delta l/l_0$) between 0.35 and 0.40. Considering that ε = e/t, the strain rate is approximately 2.5 to 3 *10^{-14} s^{-1}. This value represents a maximum strain rate value as it does not consider the possibility that shortening occurs also in other parts of the margin, like the upper slope or in the retrowedge in Puget Lowland [Johnson et al., 2004]. If the main motion along the plate boundary is controlled by great earthquakes as suggested by Wang and Hu [2006], velocity-weakening behavior would occur deeper along the megathrust surface as predicted from GPS measurements. These place the seismogenic transition zone (350–450°C at the plate interface) below the Cascadia continental shelf, with its seaward boundary situated at the shelf break [e.g., Khazaradze et al., 1999; Oleskevich et al., 1999] (Figure 1). However, this would not preclude ductile deformation at the base of the wedge occurring at lower strain rates above the megathrust surface such as modeled for brittle-ductile wedges by Williams et al. [1994]. According to these authors this zone where the decollement behaves frictionally and the base of the wedge ductilely is characterized by a steeper slope, such as observed in the Cascadia upper slope.

[29] One of the most important results we have obtained in this analysis is that we may image the plastic-brittle transition in the seismic lines we show here and that it approximately occurs below the upper slope domain (e.g., Line So107, Figure 8) at a depth between 7 and 9 km and a temperature of approximately 300°C. Consequently, the base of the prism starts deforming by dislocation creep mechanisms below the upper slope, coinciding with an important increase in the wedge slope angle, while the decollement probably still behaves frictionally [Williams et al., 1994]. The frontal part of the prism, including the landward-vergent imbricate fan, the triangular zone and the region of detached folds deforms by brittle deformation mechanisms, and also, by ductile mechanisms that require a low-activation energy, like creep by dissolution transfer [Teas et al., 1995].

6. Discussion

6.1. Thermal Gradient and Structure of the Frontal Portion of the Cascadia Accretionary Wedge

[30] Detailed analysis of the first thrust sheet in the deformation front of the accretionary wedge shows a vertical strain gradient at the base of the thrust sheet that produces a downward increase in the bedding angle of the hangingwall flat segment and second, a change in deformation mechanisms to brittle faulting in the shallower parts of the thrust sheet (Figure 4). This strain gradient probably reflects changes in the effectiveness of thermally driven deformation mechanisms like creep by dissolution transfer [Teas et al., 1995]. A loss of area is actually observed in the lowermost stratigraphic unit when restoring the first thrust to the undeformed state using GEOSEC software, most probably related with dissolution transfer processes. This strain gradient causes mechanical decoupling between the base and the upper section of the accretionary wedge, producing the basal duplex and the overlying landward-

vergent imbricated stack [*Adam et al.*, 2004]. This is an important example of how internal strain, which is not considered or measured during the balancing and restoration of shortening associated to thrusts can actually affect the larger scale structure of an accretionary wedge, as suggested by *Carminatti and Siletto* [1997].

6.2. Structure and Thermal Gradient of the Cascadia Wedge Below the Upper Slope

[31] The intermediate detachment, roof thrust of the basal duplex, can be identified in the entire lower slope terrace, in the domains of landward-vergent thrusts, in the triangular zone and forming the decollement level in the domain of detached folds. Coinciding with the base of the upper slope this fault is uplifted, warped and abandoned, being cut by the out of sequence Cascadia Main Thrust. This process may coincide with the inception of plastic deformation (dislocation creep) at the base of the wedge as shown in the strength envelope determined in this region (Figure 8). Initiation of plastic deformation at this point would explain the strong increase in the wedge slope angle to $3-5°$, as theoretically predicted by *Williams et al.* [1994] for the region at the transition between brittle and plastic behavior. The increase in slope angle is related with decoupling between the basal decollement that deforms frictionally at high-strain rates and the base of the wedge that deforms at lower strain rates by plastic creep [*Williams et al.*, 1994; *Carminati and Siletto*, 1997].

[32] Refraction data, coincident with lines So103 and So107 show a clear wedge of higher velocity material (5.0 km/s) with its tip situated below the base of the upper slope [*Flueh et al.*, 1998]. The presence of this higher-velocity material landwards from the upper-slope base was interpreted as a rigid backstop, which has not been deformed during the Quaternary accretionary phase [*Flueh et al.*, 1998]. The assumption that the growth of the Cascadia accretionary margin occurs only by frontal accretion implies that areas landwards of the deformation front are mostly tectonically inactive, especially in the upper slope, excepting the activity of normal listric faults [*McNeill et al.*, 1997, Figure 1]. However, this static interpretation of the upper slope of the Cascadia margin contrasts with other geological evidence suggesting uplift of this area during the Quaternary [*McNeill et al.*, 2000] and present [*Mazzotti et al.*, 2007]. This uplift has favored deep incision of submarine canyons in the continental slope, which breached the outer arc high [*McNeill et al.*, 2000].

[33] Adding the active uplift observed in the Cascadia upper slope to the velocity and thermal structure underlying it suggests that this region is undergoing active shortening at depth within the brittle-plastic transition, probably related to midcrustal duplex development. This is supported by the seismic images most clearly in line So109, where the basal thrust of the seaward-vergent imbricate stack is folded and uplifted when it reaches the upper slope and where the following thrusts, toward the continent, root in a shallow folded detachment. This shallow detachment may thus, represent the roof thrust of an underlying brittle-plastic duplex (Figure 3). Adding new horses to the developing

duplex uplifts the intermediate detachment and the overlying imbricate fan and may represent an important mechanism for seaward growth of the Cascadia margin.

[34] Thrust sheets evolving in a midcrustal duplex typically experience a complex deformational history, including brittle deformation during underthrusting, plastic deformation under peak burial conditions and later further frictional deformation during uplift related to forward propagation of the duplex structure [e.g., *Dunlap et al.*, 1997]. Strong internal plastic strain, generally observed in midcrustal duplexes, [*Teyssier*, 1985; *Sample and Fisher*, 1986; *Dunlap et al.*, 1997] and metamorphism followed by later freezing during uplift will result in strain hardening and development of a dynamic backstop landwards from the base of the Cascadia upper slope.

[35] Unloading driven by localized, active or recent erosion in the upper slope may have favored duplex development and associated uplift producing wide dome structures [e.g., *Konstantinovskaia and Malavieille*, 2005] imaged in the refraction seismic profiles [*Flueh et al.*, 1998; *Parsons et al.*, 1998], probably equivalent to the outer-forearc high described by *McNeill et al.* [2000] in the Oregon margin further south. Furthermore, erosion and redeposition in the lower slope is a feedback mechanism for thickening the wedge seaward from the upper slope, promoting seaward migration of the brittle-ductile transition. Out of sequence thrusts at the base of the upper slope, like the Cascadia Main Thrust, detaching in the roof thrust of the underlying duplex, may also contribute to this process. Finally, uplift associated with active underplating would explain the normal faults observed in the Cascadia upper slope [*Piper et al.*, 1995; *McNeill et al.*, 1997] that may play an important role in maintaining the critical wedge taper by compensating excess uplift [*Platt*, 1986].

6.3. Heterogeneous Deformation Along the Cascadia Margin Offshore Washington

[36] Heterogeneous deformation along the margin between landward- and seaward-vergent regions seems to be related to the proximity to the Astoria fan axial region that deforms by seaward-vergent thrusts. This may relate to changes in the lithology of the sedimentary cover such as the proportion of smectite clays diminishing toward the south [*Underwood*, 2002], to higher sand/clay ratios or/and to the existence of a thicker sedimentary cover in the axial zone of the submarine fan. The geometry of the thrusts in the frontal part of the seaward-vergent domain may be informative. They have a planar, high-angle ($\approx 50°$) geometry in their top $3-4$ km and listric geometry at depth (Figure 3). This geometry contrasts with the low angle and ramp-flat geometry of the thrusts in the sections to the north, especially section So111 (Figure 6). Ramp-flat geometry is associated to rheological contrasts between two different lithologies, like clays and sandstones, for example. While, the constant dip of the thrusts in line So109 may indicate a rather uniform lithology. A dominant sandstone lithology is supported by the abundant channels observed in the sedimentary sequence (Figure 3). Thus there may be a lithological contrast between the segment along the Astoria

submarine fan and the margin further north that would be richer in clay fraction sediments.

[37] The great thickness of the sedimentary cover in the margin segment imaged by line So109 favors an increase in the temperature at the base of the prism that reaches 250°C or more (Figure 8). The higher temperature reached in this area results in the development of a narrower wedge that undergoes plastic deformation at its base only 35 to 40 km away from the deformation front. Moreover, the high-angle thrusts in this part of the margin are not very effective producing shortening of the margin, accounting only for 11% shortening in the frontal 35 km (Figure 6). Layer parallel shortening is more effective in competent rocks like sandstones that show higher characteristic fold amplitudes [*Ramsay and Huber*, 1987], thus, thickening of individual layers has probably made a greater contribution to shortening this part of the margin. This heterogeneous deformation in the frontal part of the margin between the landward- and seaward-vergent regions is accommodated by lateral NW/SE-oriented sinistral transfer faults. These faults must transfer shortening accommodated by the landward-vergent imbricate stack to the north to crustal thickening produced by underplating below the upper slope in regions to the south.

7. Conclusions

[38] The combined analysis of structure, BSR-derived heat flow, thermal gradient and strength of the Cascadia accretionary wedge suggests a strong relationship between the thermal gradient and the mechanics, structure and tectonic evolution of the prism. The downward extrapolation of the BSR-derived thermal gradient to the base of the prism indicates temperatures between 150–200°C and 250–300°C at the deformation front and the base of the upper slope, respectively. This elevated thermal gradient affects the structure of the prism, changing the structural style, both in depth and along the convergence direction.

[39] The thermally activated strain gradient at the base of the accretionary wedge at the deformation front contributes

to the particular structure of the Cascadia margin characterized by a landward vergent imbricated thrust fan overlying a seaward vergent basal duplex. The intersection of the brittle-ductile transition with the base of the wedge at relatively shallow depths of 7–9 km under the Cascadia upper slope may also influence the geometry of the accretionary wedge, contributing to an increase in the surface angle of the upper slope. This slope increase is probably related with mechanical decoupling between the base of the wedge that deforms by dislocation creep mechanisms and the decollement that behaves frictionally during great earthquakes [*Williams et al.*, 1994].

[40] We have measured strong variations in the amount of shortening of the frontal part of the accretionary wedge between landward and seaward-vergent segments of the margin. Shortening related to thrusting in the landward-vergent regions reaches 30%, while in the seaward vergent zone further south we have only measured 11% shortening. Part of the shortening to the north seems to be transferred by sinistral transfer faults to regions thickening by crustal underplating under the upper slope in the seaward-vergent zone. Underplating by brittle-ductile duplex development below the Cascadia upper slope is an important process driving uplift, erosion and local extension of the Cascadia margin offshore Washington. This region, thus, is tectonically active and is determinant in the seaward growth and development of the Cascadia margin.

References

Adam, J., D. Klaeschen, N. Kukowski, and E. Flueh (2004), Upward delamination of Cascadia Basin sediment infill with landward frontal accretion thrusting caused by rapid glacial age material flux, *Tectonics*, *23*, TC3009, doi:10.1029/2002TC001475.

Barnard, W. D. (1973), Late Pleistocene deformation of Cascadia Basin turbidites along Washington continental margin, *AAPG Bull.*, *57*, 768–769.

Blackwell, D. D., J. L. Steele, S. Kelley, and M. A. Korosec (1990), Heat flow in the State of Washington and thermal conditions in the Cascade Range, *J. Geophys. Res.*, *95*, 19,495–19,516.

Bollinger, G. A., P. Henry, and J. P. Avouac (2006), Mountain building in the Nepal Himalaya: Thermal and kinematic model, *Earth Planet. Sci. Lett.*, *244*, 58–71.

Bonini, M. (2007), Deformation patterns and structural vergence in brittle-ductile thrust wedges: An additional analogue modelling perspective, *J. Struct. Geol.*, *29*, 141–158.

Brace, W. F., and J. D. Byerlee (1970), California earthquakes: Why only shallow focus?, *Science*, *168*, 1573–1575.

Brace, W. F., and D. L. Kohlstedt (1980), Limits on lithospheric stress imposed by laboratory experiments, *J. Geophys. Res.*, *85*(B11), 6,248–6,252.

Burov, E., L. Jolivet, L. Le Pourhiet, and A. Poliakov (2001), A thermomechanical model of exhumation of high pressure (HP) and ultra-high pressure (UHP) metamorphic rocks in Alpine-type collision belts, *Tectonophysics*, *342*, 113–136.

Byrne, D. E., W.-H. Wang, and D. M. Davis (1993), Mechanical role of backstops in the growth of forearcs, *Tectonics*, *12*, 123–144.

Carminati, E., and G. B. Siletto (1997), The effects of brittle-ductile transitions in basement-involved foreland belts: The Central Southern Alps case (N. Italy), *Tectonophysics*, *280*, 107–123.

Couzens-Schultz, B., B. Vendeville, and D. Wiltschko (2003), Duplex style and triangle zone formation: Insights from physical modeling, *J. Struct. Geol.*, *25*, 1623–1644.

Davis, D., J. Suppe, and F. A. Dahlen (1983), The mechanics of fold-and-thrust belts and Accretionary Wedges, *J. Geophys. Res.*, *88*, 1153–1172.

Davis, E. E., R. D. Hyndman, and H. Villinger (1990), Rates of fluid expulsion across the northern cascadia accretionary prism: Constraints from new heat flow and multichannel seismic reflection data, *J. Geophys. Res.*, *95*, 8869–8889.

DeMets, D., R. G. Gordon, D. F. Angus, and C. Stein (1990), Current plate motions, *Geophys. J. Int.*, *101*, 425–478.

Dickens, G. R., and M. S. Quinby-Hunt (1994), Methane hydrate stability in seawater, *Geophys. Res. Lett.*, *21*, 2115–2118.

Duncan, R. A., and L. D. Kulm (1989), Plate tectonic evolution of the Cascades arc-subduction complex, in *The Eastern Pacific Ocean and Hawaii*, edited by E. L. Winterer, D. M. Hussong, and R. W. Decker, Geol. Soc. Am., Boulder, Colo.

Dunlap, W. J., G. Hirth, and C. Teyssier (1997), Thermomechanical evolution of a ductile duplex, *Tectonics*, *16*, 983–1000.

Engebretson, D. C., A. Cox, and R. G. Gordon (1983), Relative motions between oceanic and continental plates in the Pacific Basin, in *Circum-Pacific Terrane Conference*, edited by D. G. e. a. Howell, pp. 80–82, Sch. of Earth Sci. Stanford, Stanford Univ., Calif.

Fisher, M. A., E. R. Flueh, D. W. Scholl, T. Parsons, R. E. Wells, A. Trehu, U. T. Brink, and C. S. Weaver (1999), Geologic processes of accretion in the Cascadia subduction zone west of Washington State, *J. Geodyn.*, *27*, 277–288.

Flueh, E. R., et al. (1998), New seismic images of the Cascadia subduction zone from cruise SO108-ORWELL, *Tectonophysics*, *293*, 69–84.

Ganguly, N., G. D. Spence, N. R. Chapman, and R. D. Hyndman (2000), Heat flow variations from bottom simulating reflectors on the Cascadia margin, *Mar. Geol.*, *164*, 53–68.

Goldfinger, C., L. D. Kulm, L. C. McNeill, and P. Watts (2000), Super-scale failure of the southern Oregon Cascadia margin, in *Landslides and Tsunamis*, edited by B. Keating, C. Waythomas, and A. G. Dawson, *Pure App. Geophys. Spec. Vol.*, vol. 157, pp. 1189–1226.

Govers, R., and P. T. Meijer (2001), On the dynamics of the Juan de Fuca plate, *Earth Planet. Sci. Lett.*, *189*, 115–131.

Grevemeyer, I., and H. Villinger (2001), Gas hydrate stability and the assessment of heat flow through continental margins, *Geophys. J. Int.*, *145*, 647–660.

Gutscher, M. A., D. Klaeschen, E. Flueh, and J. Malavieille (2001), Non-Coulomb wedges, wrong-way thrusting, and natural hazards in Cascadia, *Geology*, *29*, 379–382.

Gutscher, M. A., and D. C. P. Peacock (2003), Thermal models of flat subduction and the rupture zone of great subduction earthquakes, *J. Geophys. Res.*, *108*(B1), 2009, doi:10.1029/2001JB000787.

Haugerud, R. A. (1999), Digital elevation model (DEM) of Cascadia, latitude 39N-53N, longitude 116W-133W, in *Open-File Report 99-369, version 1.0*, USGS, Seattle.

Hirth, G., C. Teyssier, and W. J. Dunlap (2001), An evaluation of quartzite flow laws based on comparisons between experimentally and naturally deformed rocks, *Int. J. Earth Sci.*, *90*, 77–87.

Hyndman, R. D., and K. Wang (1993), Thermal constraints on the zone of major thrust earthquake failure: The Cascadia subduction zone, *J. Geophys. Res.*, *98*, 2039–2060.

Hyndman, R. D., and S. M. Peacock (2003), Serpentinization of the forearc mantle, *Earth Planet. Sci. Lett.*, *212*, 417–432.

Hyndman, R. D., and K. Wang (1995), The rupture zone of Cascadia great earthquakes from current deformation and the thermal regime, *J. Geophys. Res.*, *100*, 22,133–22,154.

Johnson, Y. S., R. J. Blakely, W. J. Stephenson, S. V. Dadisman, and M. A. Fisher (2004), Active shortening of the Cascadia forearc and implications for seismic hazards of the Puget Lowland, *Tectonics*, *23*, TC1011, doi:10.1029/2003TC001507.

Khazaradze, G., A. Qamar, and H. Dragert (1999), Tectonic deformation in western Washington from continuous GPS measurements, *Geophys. Res. Lett.*, *26*, 3153–3156.

Kohlstedt, D. L., B. Evans, and S. J. Mackwell (1995), Strength of the lithosphere constraints imposed by laboratory experiments, *J. Geophys. Res.*, *100*, 17,587–17,602.

Konstantinovskaia, E., and J. Malavieille (2005), Erosion and exhumation in accretionary orogens: Experimental and geological approaches, *Geochem. Geophys. Geosyst.*, *6*, Q02006, doi:10.1029/2004GC000794.

MacKay, M. E. (1995), Structural variation and landward vergence at the toe of the Oregon accretionary prism, *Tectonics*, *14*, 1309–1320.

Mazzotti, S., A. Lambert, N. Courtier, L. Nykolaishen, and H. Dragert (2007), Crustal uplift and sea level rise in northern Cascadia from GPS, absolute gravity, and tide gauge data, *Geophys. Res. Lett.*, *34*, L15306, doi:10.1029/2007GL030283.

McNeill, L. C., A. Piper, C. Goldfinger, L. V. D. Kulm, and R. S. Yeats (1997), Listric normal faulting on the Cascadia continental margin, *J. Geophys. Res.*, *102*, 12,123–12,138.

McNeill, L. C., C. Goldfinger, L. V. D. Kulm, and R. S. Yeats (2000), Tectonics of the Neogene Cascadia forearc basin: Investigations of a deformed late Miocene unconformity, *GSA Bull.*, *112*, 1209–1224.

Moore, J. C., and D. Saffer (2001), Updip limit of the seismogenic zone beneath the accretionary prism of southwest Japan: An effect of diagenetic to low-grade metamorphic processes and increasing effective stress, *Geology*, *29*, 183–186.

Oleskevich, D. A., R. D. Hyndman, and K. Wang (1999), The updip and downdip limits to great subduction earthquakes: Thermal and structural models of Cascadia, south Alaska, SW Japan, and Chile, *J. Geophys. Res.*, *104*, 14,965–14,991.

Parsons, T., A. M. Tréhu, J. H. Luetgert, K. Miller, F. Kilbride, R. E. Wells, M. A. Fisher, E. Flueh, U. S. T. Brink, and N. I. Christensen (1998), A new view into the Cascadia subduction zone and volcanic arc: Implications for earthquake hazards along the Washington margin, *Geology*, *26*, 199–202.

Piper, K. A., L. C. McNeill, and C. Goldfinger (1995), Active growth faulting on the Washington continental margin, *AAPG Bull.*, *79*, 596.

Platt, J. L. (1986), Dynamics of orogenic wedges and the uplift of high-pressure metamorphic rocks, *Geol. Soc. Am. Bull*, *97*, 1037–1053.

Ramsay, J. G., and M. I. Huber (1987), *The Techniques of Modern Structural Geology, 2: Folds and Fractures*, 307 pp., Elsevier, London.

Ranalli, G. (1995), *Rheology of the Earth*, 413 pp., CRC Press, Boca Raton, Fla.

Rybacki, E., and G. Dresen (2004), Deformation mechanism maps for feldspar rocks, *Tectonophysics*, *382*, 173–187.

Sample, J. C., and D. M. Fisher (1986), Duplex accretion and underplating in an ancient accretionary complex, Kodiak Islands, Alaska, *Geology*, *14*, 160–163.

Scholz, C. H. (1998), Earthquakes and friction laws, *Nature*, *391*, 37–42.

Seely, D. R. (1977), The significance of landward vergence and oblique structural trends on trench inner slopes, in *Island Arcs, Deep Sea Trenches and Back-Arc Basins*, edited by M. Talwani and W. C. Pitman, vol. 1, pp. 187-198, AGU, Washington, D. C.

Smit, J. H. W., J. P. Brun, and D. Sokoutis (2003), Deformation of brittle-ductile thrust wedges in experiments and nature, *J. Geophys. Res.*, *108*(B10), 2480, doi:10.1029/2002JB002190.

Teas, P. A., H. J. Tobin, and P. E. García (1995), Microstructural analysis of Sites 891 and 892: implications for deformation processes at the frontal thrust and an out-of-sequence thrust, in *Proc. ODP Pr. Sci. Res.*, edited by B. Carson et al., pp. 217–232, Ocean Drilling Program, College Station, Tex.

Teyssier, C. (1985), Crustal thrust system in an intracratonic tectonic environment, *J. Struct. Geol.*, *7*, 689–700.

Trehu, A. M., I. Asudeh, T. M. Brocher, W. D. J. H.Luetgert, J. L. Mooney, and Y. Nabelek (1994), Crustal architecture of the Cascadia Forearc, *Science*, *266*, 237–243.

Tréhu, A. M., et al. (2003), Proc. ODP, Init. Repts., 204 [CD-ROM], 77845-9547, Ocean Drill. Program, Texas A&M Univ., College Station, Tex.

Underwood, M. B. (2002), Strike-parallel variations in clay minerals and fault vergence in the Cascadia subduction zone, *Geology*, *30*, 155–158.

Underwood, M. B., K. D. Hoke, A. T. Fisher, E. E. Davis, E. Giambalvo, L. Zühlsdorff, and G. A. Spinelli (2005), Provenance, stratigraphic architecture, and hydrogeologic influence of turbidites on the mid-ocean flank of northwestern Cascadia basin, Pacific Ocean, *J. Sediment. Res.*, *75*, 149–164.

Wang, K. (2000), Stress-strain "paradox", plate coupling, and forearc seismicity at the Cascadia and Nankai subduction zones, *Tectonophysics*, *319*, 321–338.

Wang, K., and Y. Hu (2006), Accretionary prisms in subduction earthquake cycles: The theory of dynamic Coulomb wedge, *J. Geophys. Res.*, *111*, B06410, doi:10.1029/2005JB004094.

Williams, C. A., C. Connors, F. A. Dahlen, E. J. Price, and J. Suppe (1994), Effect of the brittle-ductile transition on the topography of compressive mountain belts on Earth and Venus, *J. Geophys. Res.*, *99*, 19,947–19,974.

Wilson, D. S. (1993), Confidence intervals for motion and deformation of the Juan de Fuca plate, *J. Geophys. Res.*, *88*, 16,053–16,071.

Wintsch, R. P., and K. Yi (2002), Dissolution and replacement creep: A significant deformation mechanism in mid-crustal rocks, *J. Struct. Geol.*, *24*(6–7), 1179–1193 (Micro Structural Processes: A Special Issue in Honor of the Career Contributions of R.H. Vernon).

Zhang, Y. K. (1993), The thermal blanketing effect of sediments on the rate and amount of subsidence in sedimentary basins formed by extension, *Tectonophysics*, *218*, 297–308.

———————

G. Booth-Rea, Departamento de Geodinámica, Instituto Andaluz de Ciencias de la Tierra UGR-CSIC, Avenida Fuentenueva s/n, 18002-Granada, Spain. (gbooth@ugr.es)

D. Klaeschen and I. Grevemeyer, IFM-GEOMAR, Leibnitz Institute of Marine Sciences, Wischhofstrasse 1-3, D-20148 Kiel, Germany.

T. Reston, School of Geography, Earth and Environmental Sciences, University of Birmingham, Edgbaston, Birmingham B15 2TT, UK.